Design of a High-Robustness Flap Skew Detection Monitoring Threshold

TIAN Jinqiang[1,2*], *TONG Mingbo*[2], *XUE Ying*[1]

1. Shanghai Aircraft Design and Research Insititute, Shanghai 200210, P. R. China; 2. College of Aerospace Engineering, Nanjing University of Aeronautics and Astronautics, Nanjing 210016, P. R. China

(Received 1 August 2025; revised 28 September 2025; accepted 26 November 2025)

Abstract: Focusing on civil aircraft flap skew detection design, this paper proposes a high-robustness monitoring design methodology to address insufficient monitor robustness that may trigger false alarms and disrupt airline operations. Based on flap skew detection principles and threshold design criteria, the threshold range is defined with upper limit of maximum deformation under aerodynamic load and lower limit of sensor error margin and nominal flight deformation. Since the complex loading conditions of maximum flap differential deformation (max $\Delta\lambda$) during normal flight cannot be theoretically determined, probabilistic methods are employed: Flight test data from hundreds of sorties are analyzed using generalized extreme value distribution. Confidence levels are verified via Kolmogorov-Smirnov (K-S) hypothesis testing. Then probability density function of max $\Delta\lambda$ is established. The false alarm rate is calculated through cumulative probability values of max $\Delta\lambda$ at varying thresholds. Boundary conditions for false alarm rate are determined by safety assessment and dispatch reliability analysis. The derived monitoring threshold is verified against finite element analysis predictions and iron bird rig test. The results confirm the methodology's validity, meeting all design objectives.

Key words: flap; skew detection; extreme distribution; hypothesis test; false alarm rate

CLC number: TN925 **Document code:** A **Article ID:** 1005-1120(2026)01-0073-12

0 Introduction

Modern civil aircraft high lift system consists of slat and flap. During takeoff and landing, it increases the aircraft's lift at low speeds by extending the flaps/slats to alter the wing's curvature and camber. The pilot operates the flap/slat control lever to the commanded position, and the lever signal is transmitted via cables to the flap control unit. The control channel calculates and generates control commands to actuate the power drive unit, which drives the transmission system to transfer torque and rotation to the actuators. The actuators then extend or retract the surfaces, ensuring synchronized movement of the flap and slat. Wingtip position sensors which are installed at the end of the transmission system feedback the surface position to the controller, enabling precise control to reach the required position. The surfaces are locked in place by a motor brake once the commanded position is achieved. The wingtip brake locks the system when the surfaces are fully retracted to the zero position or when a system malfunction requires shutdown[1]. The architecture of high lift system is shown in Fig.1.

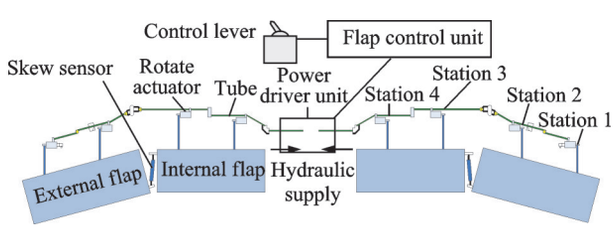

Fig.1 A typical high lift flap system architecture

Flap skew is a failure mode that occurs in a centrally driven system with torque tubes and gear transmission. When a pulley-rail mechanism, a link-

*Corresponding author, E-mail address: tianjinqiang@comac.cc.

How to cite this article: TIAN Jinqiang, TONG Mingbo, XUE Ying. Design of a high-robustness flap skew detection monitoring threshold[J]. Transactions of Nanjing University of Aeronautics and Astronautics, 2026, 43(1): 73-84.

http://dx.doi.org/10.16356/j.1005-1120.2026.01.006

rocker mechanism, or a gear-rack mechanism at a certain station of the flap disengages or jams, the flap may skew due to aerodynamic loads or continued driving force from another actuator on the same surface, as shown in Fig.2. Flap skew can create a step difference between adjacent flap panels. If this step difference exceeds a certain threshold, it may generate significant rolling moments that cannot be balanced by the opposite aileron, spoilers, or other control surfaces. Additionally, it could lead to structural damage on the wing surface[2].

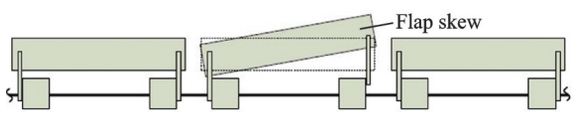

Fig.2 Flap skew diagram

The high lift system is equipped with a flap skew sensor linear variable differential transformer (LVDT) on each side between the inboard and outboard flaps. The skew condition of the flaps is detected by comparing the displacement difference of the LVDTs on the left and right sides. During normal operation, even the movement of the inboard and outboard flap surfaces of one side is similar, there will still be some slight variations by the complicated cases such as temperature, vibration, … causing LVDT extension length. It will impact the accuracy of skew detection if detecting by one side LVDT only.

However, for the left and right wings, the LVDT lengths remain nearly identical under normal flight phase. Therefore, skew fault detection can be performed based on the discrepancy in LVDT lengths between the two sides. When a skew occurs on one wing, its LVDT extension length deviates from the normal operational range. If the length difference between the left and right LVDTs exceeds a predetermined threshold, a skew fault is indicated[3].

The threshold selection should, in principle, exceed the lower limit of the sensor's normal range to prevent false alarms, while remaining below the upper limit of detachment deformation to avoid missed detections, as illustrated in Fig.3.

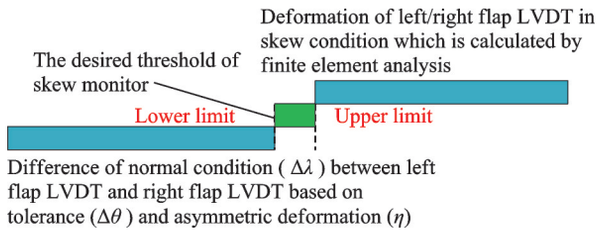

Fig.3 Threshold definition diagram

However, during the actual flight phase, the unbalance aerodynamic loads cause the asymmetric deformation in left and right wings. These deformations lead to asymmetric movement of the LVDTs of the left and right wings, resulting in discrepancies that often exceed expected values and trigger false alarms. But the finite element analysis is working based on the symmetric flight load scenarios, and connot cover the asymmetric cases. Furthermore, the deformation transmitted through the wing structure to the installation point of the skew sensor under aerodynamic loads is highly complex. This often results in an overlap between the deformation ranges of skew and normal operation, making it difficult to select an appropriate threshold. Therefore, theoretical calculation is insufficient to resolve the challenges in tilt detection.

Leao et al.[4] proposed a statistical method for threshold calculation, but failed to analyze the distribution probability of asymmetric wing deformation between the two sides. Chen et al.[5] from Northwestern Polytechnical University introduced an adaptive high-lift fault detection method, which assumed a normal distribution in fault data statistics. However, their approach failed the hypothesis test when applied to the measured data in this study, rendering it unsuitable for the scenario discussed here. Richter et al.[6] from Airbus suggested a skew detection method based on wingtip rotation speed differences, which differed from the position-based LVDT approach adopted in this paper. Ma et al.[7] from Civil Aviation University of China employed the Monte Carlo method to predict flap skew distribution probability, but our practical tests revealed that it could not account for occasional in-flight asymmetric deformation effects. Han et al.[8] from AVIC discussed key considerations for flap skew threshold determination but did not provide a solution for analyzing unexpected asymmetric flap defor-

mation during flight. Wang[9] conducted simulation-based research on flap skew but did not elaborate on how to determine monitoring thresholds. Baldo et al.[10] from School of Aerospace Engineering at Universidad Politécnica de Madrid (UPM) studied an asymmetric flap detection method, However, this method only analyzed the differences in flap positions on both wings based on the precision of the flap mechanism, without considering the effects of aerodynamic deformation. Belmonte et al.[11] from Polytechnic University of Turin designed a PID controller to monitor asymmetric flap faults. However, the PID controller only simulated parameters such as the rotation speed, torque, and precision of the flap mechanism itself, without accounting for asymmetric deformation under real load conditions. The same analysis is also used by Borello et al.[12] from Polytechnic University of Turin.

Based on the above, no methods have been found in the existing domestic and international literature that can solve the practical engineering problem addressed in this paper. Therefore, this paper focuses on the selection of monitoring thresholds for flap skew detection, with particular emphasis on developing an analytical methodology that accounts for unanticipated asymmetric load conditions between the two wing sides. The research process of this study is shown in Fig.4.

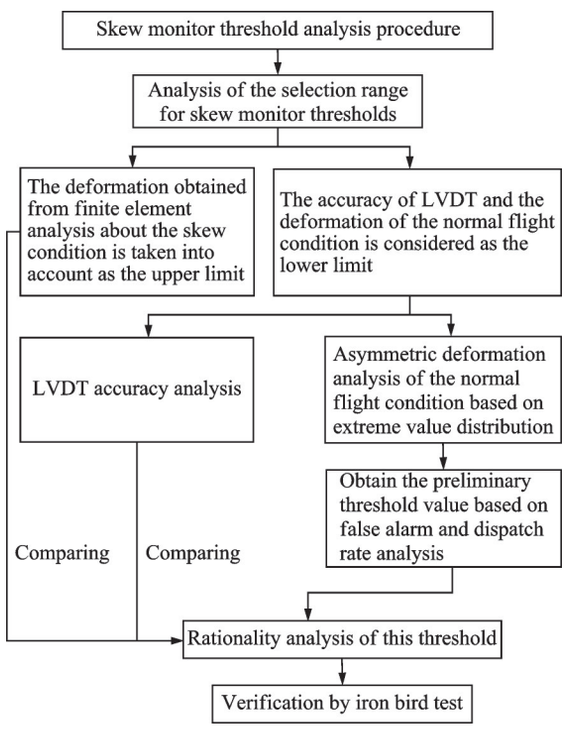

Fig.4 Flap skew monitor design diagram

1 Range of Threshold Definition

1.1 Deformation after flap skew

The design process of the flap actuation system involves multidisciplinary interactions and trade-offs across aerodynamics, structures, mechanisms, and control systems. In this study, a natural-grid finite element model based on the equivalence principles of stiffness and mass distribution is developed for the wing box, flap, and their associated actuation mechanisms. The force transfer characteristics of the flap mechanism and control system constraints are constructed to simulate the physical connections such as spherical joints and roller carriage rolling contacts between moving components. When any one of the four flap actuators losses its torque transmission capacity and rotational constraint, the flap surface will undergo skew motion under aerodynamic load until it reaches a mechanical equilibrium and stops.

The finite element analysis process consists of the following scenarios:

(1) Normal flight scenario: Under specified flight loads, the structural stress and deformations of the flap and wing box are calculated using implicit static nonlinear analysis.

(2) Skew failure scenario: Building upon scenario 1, when a single flap actuator is disconnected, the surface will be skewed due to aerodynamic forces.

(3) Various aircraft attitudes, such as pitch, roll, yaw, and sideslip, are considered to calculate the deformations under these loading scenarios.

The following separate finite element models are established for normal flight load without skew for each flap detent and normal flight load with skew for each detent. The deformations is calculated as the corresponding LVDT locations, as illustrated in Fig.5[13].

The finite element analysis yields the deformation at the LVDT mounting points of the flaps under all load conditions, thereby enabling the calculation of the minimum deformation difference between the LVDTs on the skewed side and the normal side.

The results are summarized in Table 1 below and the stations are expressed as Fig.3.

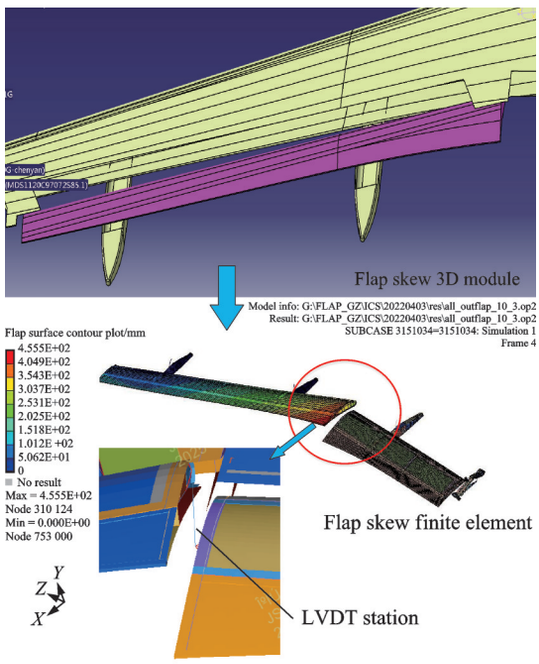

Fig.5 Finite element of flap skew

Table 1 The minimum difference between left/right LVDTs mm

Flight cycle	Flap detent	No skew	Station 1 skew	Station 2 skew	Station 3 skew	Station 4 skew
From detent 0 to 4 and back to 0	Det 0	0	4.78	−79.90	21.39	−1.56
	Det 1	0	19.50	−186.43	548.02	−83.17
	Det 1+F	0	12.69	−99.17	232.06	−29.84
	Det 2	0	7.38	−34.53	78.17	−10.09
	Det 3	0	2.99	−10.70	20.25	−2.01
	Det 4	0	−1.52	0.63	−22.01	7.80

Note: 1+F is a specific detent which is typically used during the takeoff phase to provide high lift and low drag. If the pilot moves the lever to the "1" position, the system will automatically extend the slats, and the flaps will also extend slightly, i.e., the flaps are extended to position "1" and the slats are fully extended.

The fault can be detected if the monitor threshold is set to exceed the maximum deformation value observed in any operational condition during a complete flight cycle.

1.2 Normal deformation without skew

The analysis of the normal operational range for flap LVDTs must account for two critical factors: The tolerance range of LVDT and the asymmetric deformation induced by aerodynamic loads on both wing surfaces.

The calculation method for determining the normal deformation discrepancy (without skew) $\Delta\lambda$ is expressed by

$$\Delta\lambda = \Delta\theta + \eta \tag{1}$$

where $\Delta\theta$ is the error between left and right LVDTs in normal flight phase and η the aerodynamic load-induced asymmetric deformation.

The tolerance $\Delta\theta$ induced by normal flight phase is given by

$$\Delta\theta = |\theta_{\text{left}} - \theta_{\text{right}}| \tag{2}$$

The tolerance for the left LVDT θ_{left} and right LVDT θ_{right} are expressed as

$$\theta_{\text{left}} = \theta_{\text{right}} = \pm\sqrt{\theta^2_{\text{accuracy}} + \theta^2_{\text{installation}}} \tag{3}$$

where LVDT accuracy is θ_{accuarcy} (including sensor accuracy and signal demodulation tolerance) and sensor installation tolerance is $\theta_{\text{installation}}$.

Thus, the discrepancy $\Delta\theta$ between the left and right LVDTs is calculated by

$$\Delta\theta = |\theta_{\text{left}} - \theta_{\text{right}}| = \left|2\sqrt{\theta^2_{\text{accuracy}} + \theta^2_{\text{installation}}}\right| \tag{4}$$

The known parameters in these equations are listed in Table 2.

Table 2 The minimum difference between left/right LVDTs mm

Parameter	Range
Sensor accuracy	−8.72—8.72
Installation tolerance	−3.5—3.5

Therefore, the accuracy result is 17.44 mm, the installation tolerance result is 7 mm, and the total discrepancy by root-sum-square (RSS) is 12.51 mm.

For the aerodynamic load-induced asymmetric deformation term η in Eq.(1), the flight conditions cannot be simulated clearly because the actual flight is extreme complexity. Therefore, this study employs a statistics approach to calibrate $\Delta\lambda$ based on actual flight test data. The detailed methodology presented in subsequent sections.

2 Threshold Calibration

2.1 Probability distribution of Max Δλ

This study analyzes LVDT data from 200 flight cycles (left and right channels). The left and right LVDT signals are subtracted to obtain the differential value (Δλ), then the point with the maximum differential value (max Δλ) is selected as shown in Fig.6.

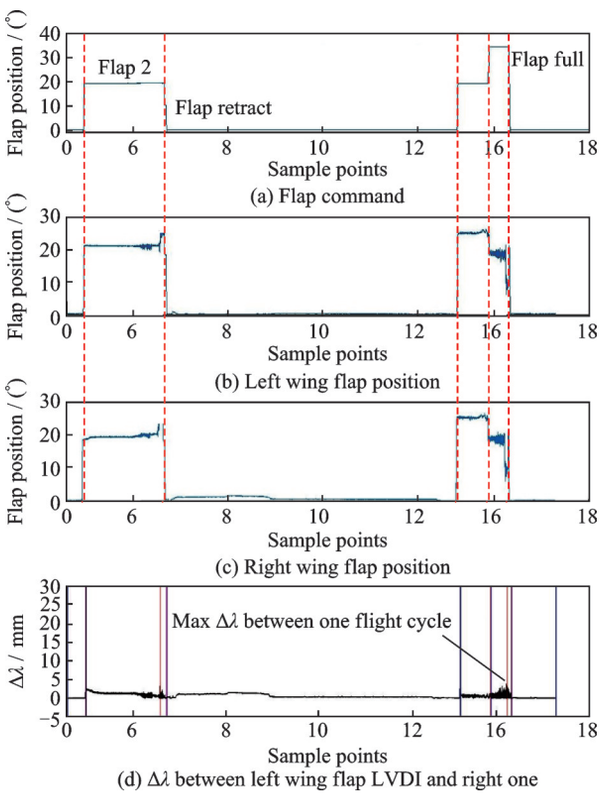

Fig.6 Actual LVDT data of in one flight test cycle

The maximum differential values (max Δλ) from all 200 flights are statistically analyzed, yielding a mean value (μ) of 7.91 mm and a standard deviation (σ) of 1.59 mm. The values are distributed within a range of 4.6 mm to 14.2 mm, with the vast majority concentrated between 6 mm and 8 mm. The corresponding histogram is shown in Fig.7.

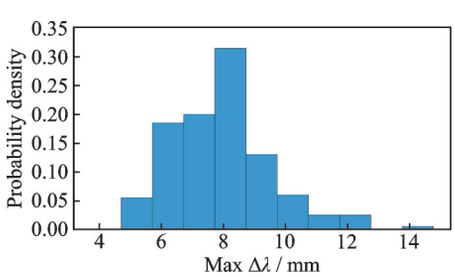

Fig.7 Probability distribution of max Δλ in 200 times flight test

Subsequently, an appropriate probability distribution must be selected for the histogram of maximum Δλ values to determine the probability density within specific monitor threshold. This study adopts the extreme value distribution.

2.2 Probability distribution analysis

The extreme value distribution refers to the probability distribution of maxima (or minima) in probability theory. It describes the probability density function $F(x)$ that should be obeyed by the extreme maximum values selected from a large number of mutually independent observations. In this article, the research focuses on the maximum difference between the two sides, so the extreme value distribution is chosen as the probability density function.

In practical applications, the distribution function $F(x)$ of random variables is often unknown, making it difficult to apply directly in statistical analysis. To estimate the distribution function of the original sample, it is essential to consider the limiting distribution as $n\to\infty$, known as the asymptotic extreme value distribution or simply the extreme value type distribution[14].

Extreme value theory has mathematically proven that there exist three types of asymptotic distributions for continuous random variables: Gumbel distribution (Eq.(5)), Fréchet distribution (Eq.(6)), and Weibull distribution (Eq.(7)).

$$f(x)=\exp\left[-\exp\left(-\frac{x-\beta}{\alpha}\right)\right]$$
$$-\infty<x<+\infty;\alpha>0 \tag{5}$$

$$f(x)=\exp\left\{-\left(\frac{(x-\beta)}{\alpha}\right)^{-k}\right\}$$
$$\beta\leqslant x\leqslant\infty;\alpha,k>0 \tag{6}$$

$$f(x)=\exp\left\{-\left(\frac{(x-\beta)}{\alpha}\right)^{k}\right\}$$
$$-\infty<x\leqslant\beta;\alpha,k>0 \tag{7}$$

where α represents the scale parameter, β the location parameter, and k the shape parameter.

Jekinson unified these three types of extreme value distributions into one, proposing the generalized extreme value (GEV) distribution to collectively represent the aforementioned extreme value distri-

butions. The calculation formula for the GEV distribution function[15] is

$$f(x)=\exp\left\{-\left[1+k\frac{(x-\beta)}{\alpha}\right]^{-\frac{1}{k}}\right\}$$

$$1+k\frac{x-\beta}{\alpha}>0 \tag{8}$$

When the shape parameter $k>0$, the GEV corresponds to Fréchet distribution; when $k=0$, it represents Gumbel distribution; and when $k<0$, it describes Weibull distribution.

The accuracy of statistical analysis results primarily depends on three factors: The probability model, the data sample, and the parameter estimation method. The choice of an appropriate parameter estimation method significantly impacts the final estimation results. The maximum likelihood estimation (MLE) method is the most commonly used parameter estimation approach in extreme value statistical analysis[16].

The likelihood function L for GEV distribution is given by

$$L(\alpha,\beta,k)=$$

$$-n\ln\alpha-\left(1+\frac{1}{k}\right)\sum_{i=1}^{n}\ln\left(1+k\frac{x_i-\beta}{\alpha}\right)-$$

$$\sum_{i=1}^{n}\ln\left(1+k\frac{x_i-\beta}{\alpha}\right)^{-\frac{1}{k}} \tag{9}$$

Construct the first-order partial derivatives of the above expression, shown as Eq.(10). α, β, and k can be computed by it.

$$\frac{\partial L}{\partial\alpha}=0,\frac{\partial L}{\partial\beta}=0,\frac{\partial L}{\partial k}=0 \tag{10}$$

To solve these equations, the Newton-Raphson iterative method is adopted in this paper, with the corresponding iterative matrix formulated in

$$\begin{pmatrix}\alpha_{\text{new}}\\ \beta_{\text{new}}\\ k_{\text{new}}\end{pmatrix}=\begin{pmatrix}\alpha_{\text{old}}\\ \beta_{\text{old}}\\ k_{\text{old}}\end{pmatrix}-\boldsymbol{H}^{-1}\nabla\boldsymbol{G} \tag{11}$$

where matrix $\boldsymbol{H}$ denotes the Hessian matrix, whose definition is given by

$$\boldsymbol{H}=\begin{pmatrix}\frac{\partial^2 L}{\partial\alpha^2} & \frac{\partial^2 L}{\partial\alpha\partial\beta} & \frac{\partial^2 L}{\partial\alpha\partial k}\\ \frac{\partial^2 L}{\partial\alpha\partial\beta} & \frac{\partial^2 L}{\partial\beta^2} & \frac{\partial^2 L}{\partial\beta\partial k}\\ \frac{\partial^2 L}{\partial\alpha\partial k} & \frac{\partial^2 L}{\partial\beta\partial k} & \frac{\partial^2 L}{\partial k^2}\end{pmatrix} \tag{12}$$

$\boldsymbol{G}$ is the gradient vector, defined as

$$\nabla\boldsymbol{G}=\begin{pmatrix}\frac{\partial L}{\partial\alpha}\\ \frac{\partial L}{\partial\beta}\\ \frac{\partial L}{\partial k}\end{pmatrix} \tag{13}$$

For equation simplification, define as

$$z_i=\frac{x_i-\beta}{\alpha} \tag{14}$$

$$y_i=\frac{1}{k}\ln(1+kz_i) \tag{15}$$

The first-order partial derivatives of α, β, and k with respect to L are given by

$$\frac{\partial L}{\partial\alpha}=\sum_{i=1}^{n}\left[-\frac{1}{\alpha}+\frac{(1+k-\mathrm{e}^{-y_i})z_i}{\alpha(1+kz_i)}\right] \tag{16}$$

$$\frac{\partial L}{\partial\beta}=-\sum_{i=1}^{n}\left[\frac{1+k-\mathrm{e}^{-y_i}}{\alpha(1+kz_i)}\right] \tag{17}$$

$$\frac{\partial L}{\partial k}=\sum_{i=1}^{n}\left[y_i+(1+k-\mathrm{e}^{-y_i})\left(\frac{z_i}{k(1+kz_i)}+\frac{y_i}{k}\right)\right] \tag{18}$$

The second-order partial derivatives of α, β, and k with respect to L are expressed in

$$\frac{\partial^2 L}{\partial\alpha^2}=\left[\frac{1}{\alpha^2}-\frac{2(1+k-\mathrm{e}^{-y_i})z_i}{\alpha^2(1+kz_i)}+\frac{(1+k-(1+kz_i)\mathrm{e}^{-y_i})z_i^2}{\alpha^2(1+kz_i)^2}\right] \tag{19}$$

$$\frac{\partial^2 L}{\partial\beta^2}=-\sum_{i=1}^{n}\left[\frac{1+k-(1+kz_i)\mathrm{e}^{-y_i}}{\alpha^2(1+kz_i)^2}\right] \tag{20}$$

$$\frac{\partial^2 L}{\partial k^2}=-\left[\frac{2y_i}{k^2}-\frac{2z_i}{k^2(1+kz_i)}-\frac{(1+k-\mathrm{e}^{-y_i})z_i^2(2+kz_i)}{k^2(1+kz_i)^2}\right] \tag{21}$$

$$\frac{\partial^2 L}{\partial\beta\partial\alpha}=\left[\frac{z_i(1+k-(1+kz_i)\mathrm{e}^{-y_i})(2+kz_i)}{\alpha^2(1+kz_i)^2}-\frac{1+k-\mathrm{e}^{-y_i}}{\alpha^2(1+kz_i)}\right] \tag{22}$$

$$\frac{\partial^2 L}{\partial\beta\partial k}=\sum_{i=1}^{n}\left[-\frac{1+k-(1+kz_i)\mathrm{e}^{-y_i})}{\alpha k(1+kz_i)^2}-\frac{1}{\alpha(1+kz_i)}\right] \tag{23}$$

$$\frac{\partial^2 L}{\partial\alpha\partial k}=\sum_{i=1}^{n}\left[-\frac{z_i(1+k-(1+kz_i)\mathrm{e}^{-y_i})}{\alpha k(1+kz_i)^2}-\frac{z_i}{\alpha(1+kz_i)}\right] \tag{24}$$

By substituting the flight test data into these equations, the estimated parameters are obtained as $\alpha = 1.352\ 3$, $\beta = 7.221\ 5$, and $k = -0.072$.

Meanwhile, based on the statistical sample mean of 7.91 mm and standard deviation of 1.59 mm, this article also introduces the normal distribution (ND) as the probability density function for the sample for comparative purposes.

The GEV probability distribution curve which is calculated by Eq.(8) is illustrated in Fig.8 (red line). And ND curve is expressed in green line.

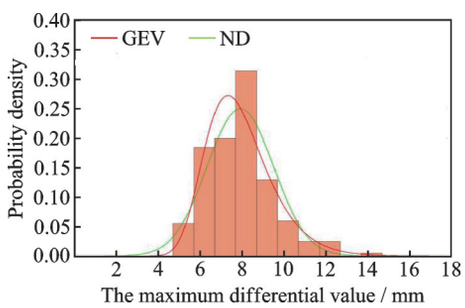

Fig.8 GEV and ND curves of max $\Delta\lambda$ in 200 times flight test

Fig.9 presents the sample cumulative density, GEV and ND cumulative density.

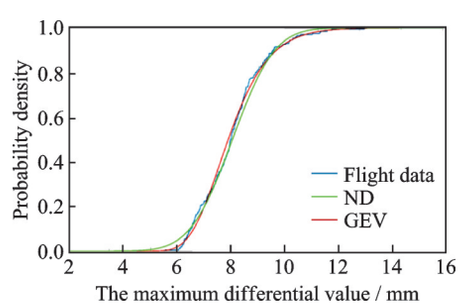

Fig.9 Max $\Delta\lambda$ sample, GEV and ND cumulative curves

To assess the fitting performance between ND and GEV, this article examines the distribution function by using the cumulative probability Kolmogorov-Smirnov (K-S) test[17]. In line with the characteristics of the K-S test method, the distribution tests are all conducted at a significance level of 0.05 (95% confidence level). The obtained p-value of GEV is 0.446 1 and the one of ND is 0.201 7, so the result indicate GEV is more appropriately distribution to represent of max $\Delta\lambda$.

2.3 False alarm rate analysis

The monitor threshold can be determined through comprehensive consideration of probability derived from the probability density function, tolerance range and finite element calculation results. The strict thresholds induce that the normal signal will be set as invalid and trigger the flap locking erroneously. The false alarm rate P_{fa} is formally expressed as

$$P_{fa} = \int_{\text{threshold}}^{\infty} P(\max \Delta\lambda)\, \mathrm{d}_{\max \Delta\lambda} \tag{25}$$

Based on Eqs.(10, 11), the curves of max $\Delta\lambda$ distribution could be calculated, as shown in Fig.10. The point of the false alarm line represents the recommended threshold value.

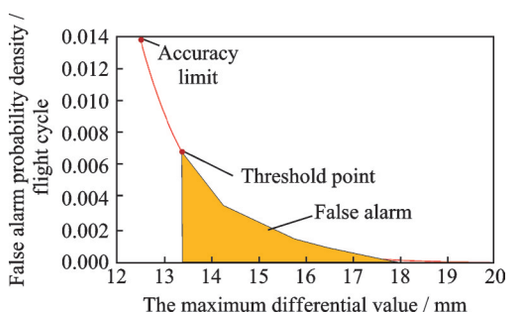

Fig.10 Probability distribution of false alarm

3 Threshold Boundary Conditions

3.1 Safety requirement

The appropriate monitoring threshold is defined based on two critical boundary conditions: System safety requirements and aircraft dispatch reliability. Excessive false alarm rates will reduce dispatch rates. Therefore, these two metrics serve as boundary conditions for threshold determination[18].

Since false alarms may trigger erroneous flap lock activation (rendering flaps inoperative), the associated functional hazard assessment (FHA) events for both affected systems are listed in Table 3, where Fh denotes flight hour.

Table 3 FHA events for aircraft

FHA event	Failure impact level	Failure rate
Announced loss of flap control	Level 4	(1e−3)/Fh

By incorporating the false alarm rate into the fault tree in Fig.11 and based on the top event requirement of (1e−3)/Fh and the system failure rate design value of (3.8e−5)/Fc, the allocated false alarm rate should be less than (2.98e−3)/Fc, where Fc is the flight cycle.

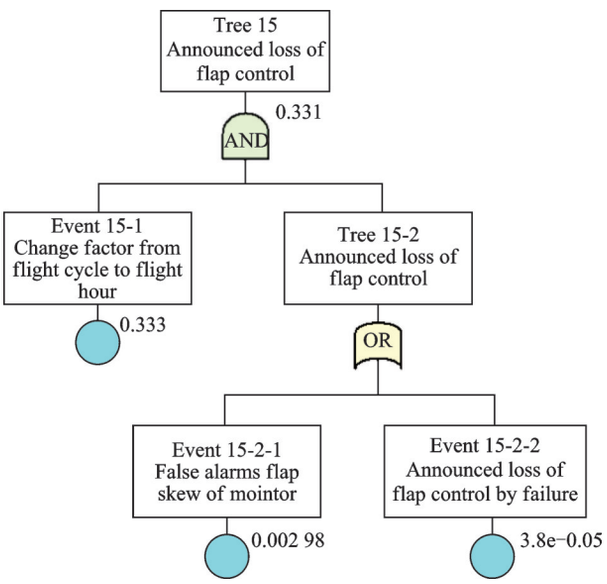

Fig.11 Announced loss of flap control fault tree

Dispatch reliability (DR) represents the proportion of successful departures without flight delays or cancellations due to technical reasons during aircraft operation. As a direct indicator of operational performance that significantly impacts aircraft economics, DR has become one of the most critical reliability metrics for airlines and stands as one of the core parameters in commercial aircraft reliability design[19].

For flight crews, when unable to verify the authenticity of an alert, it is typically treated as the truth and impact aircraft operations, thereby disrupting system operations and increasing maintenance activities[20].

3.2 Dispatch reliability requirement

The dispatch reliability calculation for a certain system is shown in

$$DR = DR_{system} + DR_{false\ alarm} \tag{26}$$

$$DR_{false\ alarm} = 1 - P_{fa} \tag{27}$$

where DR_{system} denotes the number of delays caused by system failures and $DR_{false\ alarm}$ the number of delays caused by false alarm.

For a certain aircraft type, the actual designed dispatch reliability (DR_{system}) of the high lift system is 99.962%, while the aircraft dispatch rate requirement is 99.96%. Substituting these values into Eq. (12) yields the threshold will be lower than (2e−3)/Fc.

By comparing the two values from safety analysis and dispatch reliability, the more stringent one ((2e−3/)Fc) is adopted. Then this value is applied to Fig.10, the corresponding threshold range should be greater than 14.9 mm. For practical implementation, this study adopts 15 mm as the monitoring threshold.

4 Threshold Boundary Conditions

4.1 Finite element verification

In order to verify whether the proposed threshold (15 mm) can meet the skew detection requirements, this article analysis the finite element result. The threshold is applied to Table 1 to verify whether it can cover the deformation under tilt failure conditions.

By comparing the pre-selected monitoring threshold of 15 mm with the deformation values in Table 1, the analysis results shown in Table 4 can be obtained (the skew case which can be detected is marked green). Therefore, it can be confirmed that the monitoring threshold derived from the above analysis is capable of covering skew failure scenarios during a single flight cycle.

4.2 Physical iron-bird test verification

To further verify the rationality of the threshold, this article conducts development tests based on a physical iron-bird test platform. The architecture of the iron-bird test platform is shown in Fig.12[21].

The flap skew is simulated by disconnecting the actuator at a specified station, while applying aerodynamic loads through loading actuators. The operational methodology is illustrated in Fig.13.

Table 4 Comparison of threshold and deformation

Flap detent	Station 1 skew	Station 2 skew	Station 3 skew	Station 4 skew
0	4.78<15	−79.9>15	21.39>15	4.78<15
Is skew detected?	No	Yes	Yes	No
1	19.5>15	−186.43>15	548.02>15	−83.17>15
Is skew detected?	Yes	Yes	Yes	Yes
1+F	12.69<15	−99.17>15	232.06>15	−29.84>15
Is skew detected?	No	Yes	Yes	Yes
2	7.38<15	−34.53>15	78.17>15	−10.09<15
Is skew detected?	No	Yes	Yes	No
3	2.99<15	−10.70<15	20.25>15	−2.01<15
Is skew detected?	No	No	Yes	No
4	−1.52<15	0.63<15	−22.01>15	7.8<15
Is skew detected?	No	No	No	No
Conclusion	Skew is detected for one flight cycle.			

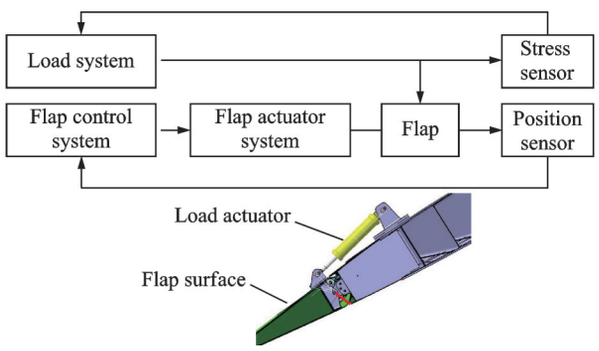

Fig.12 Flap skew detection loading test rig[21]

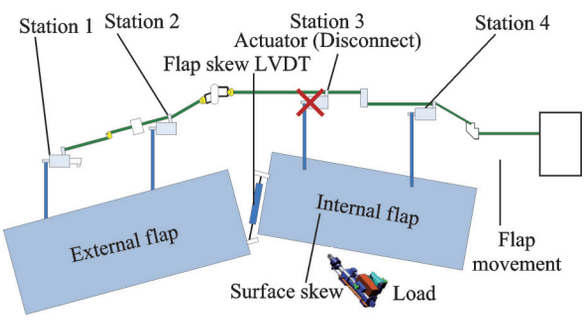

Fig.13 Flap skew detection verification methodology

The test results are presented in Table 5, the skew case which can be detected is marked green. The tests demonstrate that the monitoring threshold designed in this study can cover in-flight flap skew failures and detect them within a single flight cycle, with test results consistent with analyt-

Table 5 Skew detection test results

No	Flap operation	Load	Test result	Analysis
Station 1 skew	0—1—2—3—4 Retract to extend	No load on ground check	Trigger alarm	The skew failure in flight condition could be detected through ground inspections.
		20%load	No trigger alarm	
		50%load	Trigger alarm	
		80%load	No trigger alarm	
Station 3 skew	0—1—2—3—4 Retract to extend	No load on ground check	Trigger alarm	As expected
		20%load	Trigger alarm	
		50%load	Trigger alarm	
		80%load	Trigger alarm	
		100%load	Trigger alarm	
Station 4 skew	0—1—2—3—4 Retract to extend	No load on ground check	No trigger alarm	The skew failure in flight condition could be detected through ground inspections.
		20%load	Trigger alarm	As expected
		50%load	Trigger alarm	
		80%load	Trigger alarm	
		100%load	Trigger alarm	

Note: The case of Station 2 skew is similar with Station 3 skew because the structures of them are symmetrical, so it could be covered by Station 3 skew.

ical predictions.

It should be noted that, comparing with the load cases of finite element analysis which encompass various aircraft attitudes such as pitch, roll, yaw, and sideslip. However, due to limitations of the test rig, the iron-bird test can only simulate the aircraft in a horizontal attitude and is unable to cover other flight attitudes. Because of the strengths and limitations of both finite element analysis and physical test, this article adopts two verification methods.

5 Conclusions

This paper focuses on the flap skew detection system of commercial aircraft, proposing a design methodology for monitoring threshold determination to prevent false alarms.

Firstly, finite element analysis is conducted to calculate the theoretical deformation magnitude of the flap under tilted conditions in flight load environments.

Subsequently, the accuracy range of the flap LVDT is analyzed, along with the maximum deformation difference between each LVDT under normal conditions. To address unpredictable asymmetric flight scenarios, statistical methods are used to analyze the probability density of max $\Delta\lambda$ using data from hundreds of test flights. The GEV distribution is employed for modeling, with confidence levels validated via the K-S hypothesis test, ultimately deriving the probability density function of max $\Delta\lambda$.

Based on false alarm rate calculation principles, the cumulative probability values of max $\Delta\lambda$ at different thresholds are computed. Through system safety assessment and dispatch reliability analysis, the false alarm rate boundary conditions are determined, leading to the solution for the monitoring threshold. This target is cross-verified against theoretical finite element analysis data to ensure its validity.

The proposed monitoring threshold is verified through iron-bird flap skew test, with results meeting design expectations and confirming the methodology's validity.

The method described in this article can be applied to the threshold design of monitors that utilize sensors for fault detection. GEV is suitable for analyzing the probability distribution of the maximum values in complex signals. For monitors designed based on these signals, the false alarm rate can be determined according to the failure rate and dispatch reliability requirements of the monitored system. By substituting this false alarm rate into the probability density function of GEV, a reasonable monitor threshold can be derived.

References

[1] WANG X Y, WANG W D. A design of flap skew detection based on revolver for civil aircraft[C]//Proceedings of 2021 International Conference on Digital Society and Intelligent Systems (DSInS). Chengdu, China: IEEE, 2021: 116-120.

[2] TIAN W, CUI W M, ZHAO S J. Physical failure analysis of A320 flap based on DMU[C]//Proceedings of 2013 International Conference on Quality, Reliability, Risk, Maintenance, and Safety Engineering (QR2MSE). Chengdu, China: IEEE, 2013: 914-916.

[3] SEEHUSEN G J, EMCH G A, RENZELMANN M E. In-flight detection of wing flap free wheeling skew: US20080253747[P]. 2025-06-07.

[4] LEAO B P, GOMES J P P, GALVAO R K H, et al. Aircraft flap and slat systems health monitoring using statistical process control techniques[C]//Proceedings of 2009 IEEE Aerospace Conference. Big Sky, MT, USA: IEEE, 2009: 1-8.

[5] CHEN J, JING Z D, WU C T, et al. Improved fault diagnosis for aircraft flap control system based on bond graph[J]. Aircraft Engineering and Aerospace Technology, 2020, 92(8): 1159-1168.

[6] RICHTER M, FLEDDERMANN A. Fault-tolerant actuating system for adjusting flaps of an aircraft, comprising adjustment kinematics with a fixed pivot, and a method for monitoring an actuating system: US20110062282[P]. 2011-03-17.

[7] MA Chao, ZHANG Xiongfei, XU Jianxin. A risk prediction of aircraft flap asymmetry based on Monte Carlo method[J]. Journal of Transport Information and Safety, 2020, 38(3): 24-31. (in Chinese)

[8] HAN Sai, HUA Dongsheng. Logic of protection for flap's asymmetry movement and flap skew[J]. Advances in Aeronautical Science and Engineering,

2016, 7(1): 62-69. (in Chinese)

[9] WANG X Y. Simulation research for flap skew on a certain type of aircraft[C]//Proceedings of CSAA/IET International Conference on Aircraft Utility Systems (AUS 2024). Xi'an, China: IET, 2025: 1784-1788.

[10] BALDO L, DALLA VEDOVA M D L, CEJUDO RUIZ J M. Proposal for an enhanced monitoring technique for active control of aircraft flap asymmetry[J]. Engineering Proceedings, 2025, 90(1): 66.

[11] BELMONTE D, DALLA VEDOVA M D L, MAGGIORE P. Robust simulation model approach to evaluate innovative asymmetry monitoring and control techniques in critical flap failure and aircraft controllability[C]//Proceedings of the 6th International Conference on Theoretical and Applied Mechanics (TAM'15). Salerno, Italy: [s.n.], 2015: 133-142.

[12] BORELLO L, VILLERO G, DALLA VEDOVA M D L. Flap failure and aircraft controllability: Developments in asymmetry monitoring techniques[J]. Journal of Mechanical Science and Technology, 2014, 28(11): 4593-4603.

[13] HUANG Yong, XU Wu, ZHU Lingang, et al. Trailing-edge flap operation and asymmetric control for large passenger aircraft[J]. Tchinese Quarterly of Mechanics, 2022, 43(1): 110-121. (in Chinese)

[14] HAN Xu, WANG Jianyu, ZU Xianfeng. System maximum-error specification oriented testing methodology based on extreme value theory[J]. Systems Engineering and Electronics, 2012, 34(5): 1073-1084. (in Chinese)

[15] FENG Pengfei, ZHOU Mi, LI Zhixuan, et al. Probability statistical model for measured ground motion based on generalized extreme value distribution[J]. Journal of Shanghai Jiao Tong University, 2023, 59(8): 1133-1144. (in Chinese)

[16] CHEN Zishen, LIU Zengmei, LU Jianfei. Comparative analysis of parameter estimation methods of generalized extreme value distribution[J]. Acta Scientiarum Naturalium Universitatis Sunyatseni, 2010, 49(6): 105-109. (in Chinese)

[17] GONG Fengqiang, WANG Tiancheng, HUANG Tianlang. An inference method for probability distribution of extreme value engineering parameters based on normal information diffusion principle[J]. Journal of Central South University (Science and Technology), 2020, 51(6): 1692-1702. (in Chinese)

[18] NIU Peiyi. The failure threshold selection in fault detection of redundant control systems[J]. Acta Aeronautica et Astronautica Sinica, 1992, 13(1): 112-116. (in Chinese)

[19] CHEN Jie. Calculation of dispatch reliability of civil aircraft flight control system based on PMMEL[C]//Proceedings of the 6th Civil Aircraft Avionics International Forum. Shanghai, China: Chinese Society of Aeronautics and Astronautics Press, 2017: 204-210.

[20] PAIELLI R A, ERZBERGER H. Analysis of false-alert rates for a tactical conflict detection system[C]//Proceedings of AIAA 5th ATIO and 16th Lighter-Than-Air Sys Tech. and Balloon Systems Conferences. Arlington, Virginia: AIAA, 2005: AIAA2005-7473.

[21] WANG X Y. Test research for flap skew on iron bird on a certain type of aircraft[C]//Proceedings of CSAA/IET International Conference on Aircraft Utility Systems (AUS 2024). Xi'an, China: IET, 2024: 1789-1793.

Author

The first/corresponding author Prof. **TIAN Jinqiang** received the M.S. degree in aircraft design from Shanghai Aircraft Design and Research Institute, Shanghai, China, in 2007. In 2008, he joined the Flight Control Department of Shanghai Aircraft Design and Research Institute. Now, he works as a professor in Shanghai Aircraft Design and Research Institute. He majors in the design of fly-by-wire flight control systems, and is charge for the flight control systems design of C919.

Author contributions Prof. **TIAN Jinqiang** designed the study, complied the models, conducted the analysis, interpreted the results, and wrote the manuscript. Prof. **TONG Mingbo** was responsible for technical guidance, thesis evaluation and organizing expert reviews. Dr. **XUE Ying** contributed to the discussion and background of the study. All authors commented on the manuscript draft and approved the submission.

Competing interests The authors declare no competing interests.

(Production Editor: XU Chengting)

一种高鲁棒性襟翼倾斜探测监控器设计

田金强[1,2]，童明波[2]，薛　瀛[1]

（1.上海飞机设计研究院，上海200210，中国；2.南京航空航天大学航空学院，南京210016，中国）

摘要：本文以民用飞机襟翼倾斜探测系统为对象，针对监控器鲁棒性不足，会导致虚警影响航线运营的问题，提出了一种高鲁棒性倾斜探测监控器的设计方法。为了解决该问题，本文采用有限元分析、概率统计、故障树分析等多种方法相结合。首先根据襟翼倾斜探测的原理和阈值设计原则，确定了在翼面倾斜后最大受载下的变形量为阈值上限，以传感器误差量及正常飞行的形变量为下限的阈值范围。由于正常飞行中两侧襟翼变形量之差max Δλ所处的载荷工况较为复杂，难以通过理论计算确定，本文采用了概率统计原理，运用Gumbel极值分布律对大量试飞数据进行了分析，通过K-S假设检验确定了置信度，形成了max Δλ的概率密度函数。继而通过max Δλ的累积概率值，得到了阈值与虚警率的关系曲线。之后基于系统安全性分析和派遣率分析确定了虚警率的边界条件，根据边界条件反推计算得到监控阈值的目标解。经与有限元分析数据及铁鸟试验台襟翼倾斜试验数据比对，监控阈值的目标解得到确认，结果符合设计预期，证明了本方法的合理性。

关键词：襟翼；倾斜探测；极值分布；假设检验；虚警率

研究亮点：

1.在传统纯理论计算分析监控器阈值的基础上，创新性地提出采用极值分布概率统计法，在大量真实飞行数据中找出襟翼变形的规律，对理论计算得到的阈值进行修正。

2.基于虚警率理论，采用故障树分析和派遣率分析相结合的方法确定了虚警率的边界条件，根据边界条件反推计算得到监控阈值的目标解。